AIP Journal of Applied Physics

Step-edge-induced resistance anisotropy in quasi-free-standing bilayer chemical vapor deposition graphene on SiC

Tymoteusz Ciuk, Semih Cakmakyapan, Ekmel Ozbay, Piotr Caban, Kacper Grodecki, Aleksandra Krajewska, Iwona Pasternak, Jan Szmidt, and Wlodek Strupinski

Citation: Journal of Applied Physics **116**, 123708 (2014); doi: 10.1063/1.4896581
View online: http://dx.doi.org/10.1063/1.4896581
View Table of Contents: http://scitation.aip.org/content/aip/journal/jap/116/12?ver=pdfcov
Published by the AIP Publishing

Articles you may be interested in
Preparation and electrical transport properties of quasi free standing bilayer graphene on SiC (0001) substrate by H intercalation
Appl. Phys. Lett. **105**, 183105 (2014); 10.1063/1.4901163

Nitrogen doping of chemical vapor deposition grown graphene on 4H-SiC (0001)
J. Appl. Phys. **115**, 233504 (2014); 10.1063/1.4884015

Graphene growth on AlN templates on silicon using propane-hydrogen chemical vapor deposition
Appl. Phys. Lett. **104**, 071912 (2014); 10.1063/1.4866285

Detection of polar chemical vapors using epitaxial graphene grown on SiC (0001)
Appl. Phys. Lett. **102**, 173103 (2013); 10.1063/1.4803511

The influence of substrate morphology on thickness uniformity and unintentional doping of epitaxial graphene on SiC
Appl. Phys. Lett. **100**, 241607 (2012); 10.1063/1.4729556

[This article is copyrighted as indicated in the article. Reuse of AIP content is subject to the terms at: http://scitation.aip.org/termsconditions. Downloaded to] IP: 139.179.58.12 On: Thu, 25 Dec 2014 09:28:58

JOURNAL OF APPLIED PHYSICS 116, 123708 (2014)

Step-edge-induced resistance anisotropy in quasi-free-standing bilayer chemical vapor deposition graphene on SiC

Tymoteusz Ciuk,[1,2] Semih Cakmakyapan,[3] Ekmel Ozbay,[3] Piotr Caban,[1] Kacper Grodecki,[1] Aleksandra Krajewska,[1,4] Iwona Pasternak,[1] Jan Szmidt,[2] and Wlodek Strupinski[1,a)]
[1]Institute of Electronic Materials Technology, Wolczynska 133, 01-919 Warsaw, Poland
[2]Institute of Microelectronics and Optoelectronics, Warsaw University of Technology, Koszykowa 75, 00-662 Warsaw, Poland
[3]Department of Electrical and Electronics Engineering, Department of Physics, Nanotechnology Research Center, Bilkent University, 06800 Bilkent, Ankara, Turkey
[4]Institute of Optoelectronics, Military University of Technology, Gen. S. Kaliskiego 2, 00-908 Warsaw, Poland

(Received 14 June 2014; accepted 15 September 2014; published online 25 September 2014)

The transport properties of quasi-free-standing (QFS) bilayer graphene on SiC depend on a range of scattering mechanisms. Most of them are isotropic in nature. However, the SiC substrate morphology marked by a distinctive pattern of the terraces gives rise to an anisotropy in graphene's sheet resistance, which may be considered an additional scattering mechanism. At a technological level, the growth-preceding *in situ* etching of the SiC surface promotes step bunching which results in macro steps ~10 nm in height. In this report, we study the qualitative and quantitative effects of SiC steps edges on the resistance of epitaxial graphene grown by chemical vapor deposition. We experimentally determine the value of step edge resistivity in hydrogen-intercalated QFS-bilayer graphene to be $\sim 190\,\Omega\mu$m for step height $h_S = 10$ nm and provide proof that it cannot originate from mechanical deformation of graphene but is likely to arise from lowered carrier concentration in the step area. Our results are confronted with the previously reported values of the step edge resistivity in monolayer graphene over SiC atomic steps. In our analysis, we focus on large-scale, statistical properties to foster the scalable technology of industrial graphene for electronics and sensor applications. © *2014 AIP Publishing LLC*. [http://dx.doi.org/10.1063/1.4896581]

I. INTRODUCTION

Owing to its outstanding carrier mobility, graphene has been expected to realize high-speed electronics,[1,2] however the room-temperature carrier mobility of 140 000 cm^2/Vs was only reported for its exfoliated form on BN,[3] in excess of 15 000 cm^2/Vs on SiO_2,[4–6] and 25 000 cm^2/Vs for its suspended form[7] (200 000 cm^2/Vs at low temperature[8,9]). When graphene is grown on SiC substrate, its carrier transport is significantly affected by a range of scattering mechanisms, predominantly, long-range Coulomb scattering on charged impurities trapped in the graphene-substrate interface.[10–30] Others include short-range disorder related to intrinsic lattice imperfections, point defects and dislocations,[10,11,20,22,24–27,31–34] "ripples" in graphene's atomic structure,[6,7,35–38] and acoustic phonons.[39–41] It has been calculated that in case of monolayer graphene, the room temperature intrinsic mobility of charge carriers is phonon-limited to ~10^5 cm^2/Vs (Refs. 39–41) and the most plausible sources of scattering are charged impurities. The mean free path for short-range scatterers l_S is proportional to $1/\sqrt{n}$, where n is the charge carrier density. For Coulomb scatterers due to the screening effect, $l_S \sim \sqrt{n}$, therefore, short-range scattering must be included into formalism only for very low ionized impurity density or at high carrier densities. A simple analytic equation was derived to relate the charged-impurity-limited mobility, $\mu \times n_{imp} = 5 \times 10^{15}\,\mathrm{V}^{-1}\,\mathrm{s}^{-1}$,[14,18] where n_{imp} is the effective impurity concentration and it is suggested that reducing the typical n_{imp} in present day samples, $n_{imp} \sim 10^{11}-10^{12}\,\mathrm{cm}^{-2}$, by two orders of magnitude should increase the mobility to ~10^5 cm^2/Vs, giving way to the short-range scattering model. In bilayer graphene, the screening effect is quantitatively much stronger than in monolayer graphene. The resultant is the scattering mechanism of the over-screened Coulomb impurities which is equally important as the short-range disorder.[24,25]

In the most promising technology for wafer-scale production of graphene devices,[2,42] i.e., sublimation[43–45] and Chemical Vapor Deposition (CVD) growth on SiC,[46] surface substrate morphology also acts effectively as a scattering mechanisms. The role of SiC morphology on transport properties of graphene grown by silicon sublimation was discussed by several groups.[47–49] It has been reported that SiC step edge density,[50] step height,[51] and step bunching[52,53] give rise to graphene's resistance. The step edge resistivity in monolayer graphene was evaluated by scanning potentiometry in a scanning tunneling microscope[51] and later associated with the abrupt variation in potential and doping due to detachment of graphene from the substrate as it passes over a step.[54] Both experiments were related to SiC atomic steps and proved step edge resistivity $\rho_{step} \approx 15\,\Omega\mu$m and $\rho_{step} \approx 25\,\Omega\mu$m for step height h_s equal to 1.0 nm and 1.5 nm, respectively. Consequently, the surplus resistance introduced by step edges was explained through carrier depletion rather than an additional scattering mechanism. In Ref. 55, it is

[a)]Author to whom correspondence should be addressed. Electronic mail: wlodek.strupinski@itme.edu.pl

 © 2014 AIP Publishing LLC

[This article is copyrighted as indicated in the article. Reuse of AIP content is subject to the terms at: http://scitation.aip.org/termsconditions. Downloaded to] IP: 139.179.58.12 On: Thu, 25 Dec 2014 09:28:58

suggested that the conduction anisotropy is a reflection of both geometric anisotropy and the extent of residual silicon atoms aggregated at the step edges, where they enhance carrier scattering.

Graphene grown on Si face of SiC rests on a buffer layer which is the first layer of carbon atoms covalently bound to the substrate.[56–58] It can be decoupled to form a quasi-free-standing bilayer graphene (QFS-bilayer) through hydrogen atoms intercalation.[59] The intercalating atoms diffuse underneath the buffer layer and bound themselves to the topmost Si atoms of the SiC substrate converting the buffer layer to a mostly sp2-hybridized monolayer graphene. The resultant QFS-bilayer graphene is partly screened from the substrate and exhibits on average three times higher carrier mobility than the un-intercalated one. Importantly, its transport properties are not degraded up to 700 °C. Therefore, it is mostly suited for high-speed applications. Unfortunately, the growth-preceding *in situ* etching of the SiC surface promotes step bunching which results in macro steps ∼10 nm in height, as opposed to much lower atomic steps investigated in Refs. 51 and 54. The step bunching is expected to considerably increase the step edge resistivity. In this report, we examine the qualitative and quantitative effects of SiC steps on graphene's resistance and experimentally determine the value of ρ_{step} in hydrogen-intercalated bilayer graphene.

II. EXPERIMENTAL DETAILS

In this paper, we studied the effect of the step-edge-induced resistance anisotropy in hydrogen intercalated, QFS-bilayer graphene on the Si face of 4H-SiC(0001) and 6H-SiC(0001) (10 mm × 10 mm). The investigated samples were grown using the CVD method on semi-insulating on-axis substrates in a standard hot-wall CVD Aixtron VP508 reactor. Prior to the growth, *in situ* etching of the SiC surface was carried out in hydrogen atmosphere. The epitaxial CVD growth of graphene was realized under dynamic flow conditions that simultaneously inhibit Si sublimation and promote the mass transport of propane molecules to SiC substrate.[46] The growth process was followed by *in situ* hydrogen intercalation at 1000 °C in 900 mbar Ar atmosphere. The *as grown* samples were characterized by Hall effect measurements in *van der Pauw* geometry with the four golden probes placed in the corners of the 10 mm × 10 mm substrates. Altogether 140 4H-SiC and 60 6H-SiC samples were fabricated and investigated to assure a statistical perspective. Typical values of hole concentration obtained at room temperature were of the order of $1.3 \times 10^{13}\,\mathrm{cm}^{-2}$ and their mobility proved on average 2500 cm^2/Vs (up to 5300 cm^2/Vs).

The qualitative influence of SiC step edges resulting from step bunching on the average resistance of QFS-bilayer graphene was in the first place derived from standard Hall effect characterization in *van der Pauw* geometry with the use of an 0.55T Ecopia HMS-3000 setup. Prior to the measurement, each graphene sample was inspected under an optical microscope and assigned a specific angle of the SiC terraces configuration. The terraces appear to follow a uniform direction over the entire area of a substrate. Fig. 1(a) illustrates the adopted convention for the angle assignment.

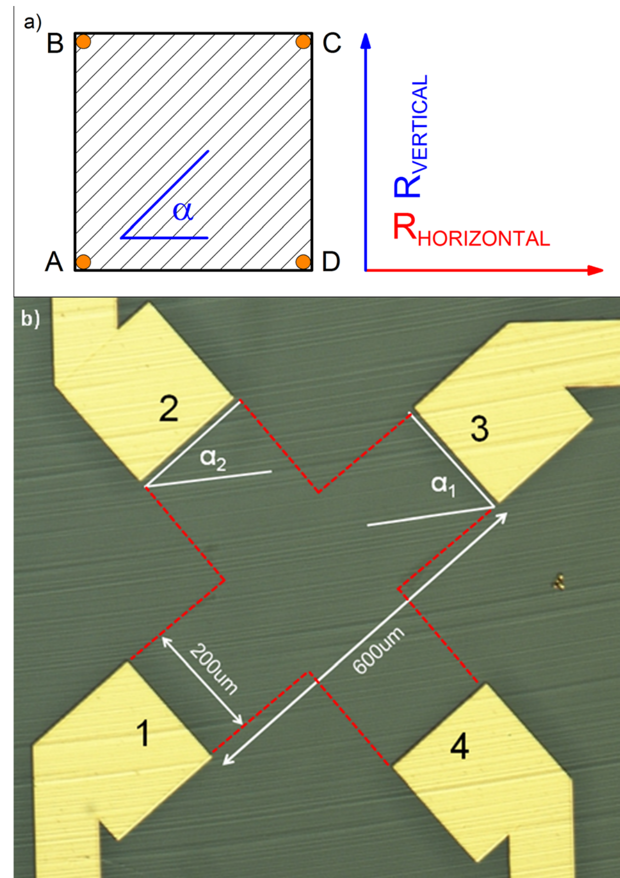

FIG. 1. (a) Schematic view of a SiC substrate (10 mm × 10 mm) and the adopted convention for the angle α assignment of the terraces orientation with respect to the SiC substrate edges. Letters A–D indicate four corners of the substrate, where the four golden pins were placed during the standard Hall effect characterization in *van der Pauw* geometry. This approach was adopted to qualitatively observe the step-edge-induced resistance anisotropy in graphene. (b) Optical image of a photolithographically patterned equal-arm graphene Hall cross designed for the quantitative analysis of the step edge resistivity.

The resultant is α ranging from 0° to 90° with the terraces running horizontally ($\alpha = 0°$), vertically ($\alpha = 90°$), or at any other angle calculated from the level.

In the standard *van der Pauw* method for the sheet resistance determination, it is required to measure the $R_{AB,CD}$, $R_{CD,AB}$, $R_{AD,BC}$, $R_{BC,AD}$, auxiliary resistances in the first place. These values are defined as $(V_D - V_C)/I_{AB}$, $(V_B - V_A)/I_{DC}$, $(V_C - V_B)/I_{AD}$, and $(V_D - V_A)/I_{BC}$, respectively. Based on this, the $R_{VERTICAL}$ and $R_{HORIZONTAL}$ are calculated as arithmetic means of ($R_{AB,CD}$, $R_{CD,AB}$) and ($R_{AD,BC}$, $R_{BC,AD}$),respectively. It can be shown that the following relation holds (van der Pauw[60]):

$$\exp\left(-\pi R_{VERTICAL}/R_S\right) + \exp\left(-\pi R_{HORIZONTAL}/R_S\right) = 1,$$

where R_S is the material's sheet resistance. In this report, the $R_{VERTICAL}$ and $R_{HORIZONTAL}$ values are considered to be influenced by the terraces orientation and are confirmed to follow a precise function of the angle α. Both resistances are related to a hypothetical $R_{AVERAGE}$ that corresponds to R_S through $2exp(-\pi R_{AVERAGE}/R_S) = 1$, where R_S is determined by $R_{VERTICAL}$ and $R_{HORIZONTAL}$. Each of the 200 verified samples was subject to two subsequent measurements

[This article is copyrighted as indicated in the article. Reuse of AIP content is subject to the terms at: http://scitation.aip.org/termsconditions. Downloaded to] IP: 139.179.58.12 On: Thu, 25 Dec 2014 09:28:58

(I = 1 mA) with the second preceded by sample rotation by 90°, thus rearranging the corners from *ABCD* to *DABC*. With this approach, our statistical perspective was doubled. The anisotropy in transport properties is manifested in normalized values of $R_{VERTICAL}/R_{AVERAGE}$ and $R_{HORIZONTAL}/R_{AVERAGE}$ in the function of α.

The qualitative observation of step-edge-induced resistance anisotropy provides a justification for further quantitative analysis. Two hydrogen intercalated QFS-bilayer 4H-SiC samples were photolithographically patterned to form nine graphene Hall bars on each. Initial *van der Pauw* characterization proved that both graphene samples displayed similar parameters: hole concentration $n \approx 1.8 \times 10^{13}\,\text{cm}^{-2}$, carrier mobility $\mu \approx 2300\,\text{cm}^2/\text{Vs}$, and sheet resistance $R_S \approx 150\,\Omega/\text{sq}$. The nine Hall bars took the form of symmetrical, equal-arm crosses rotated at a gradually increasing angle (0°, 5°, 10°, 15°, 20°, 25°, 30°, 35°, 40°) with respect to the substrate's edges and hence to SiC terraces. Each of the two bars forming the graphene cross had 200 μm in width and 600 μm in length. 20 nm_Ti/80 nm_Au ohmic contacts (200 μm × 200 μm) were e-beam deposited. Fig. 1(b) illustrates one of the nine crosses.

In order to deepen our understanding of the origin of the step edge resistivity, an additional sample with a transferred graphene was produced. Graphene grown on 12 μm thick 3N JTCHTE GOULD Electronics copper foil in Aixtron VP508 reactor was transferred onto a 4H-SiC substrate through the PMMA-mediated electrochemical delamination method.[61] Prior to transfer, the substrate underwent a process of hydrogen etching in 1600 °C to promote step bunching on its surface. An identical pattern of nine rotated Hall bars was fabricated accordingly to the above presented details.

In each of the nine Hall crosses, the specific α_1 and α_2 angles were determined. α_1 corresponds to step edge orientation in the graphene channel between contacts "1" and "3," α_2 between "2" and "4." The configuration of a Hall cross provides two mutually perpendicular graphene resistors R_{13} and R_{24}. It can be judged from the photograph that the total resistance between two opposite contact pads is described by the following formulas:

$$R_{13} = R_{C1} + R_{channel13}(\alpha_1) + R_{C3},$$
$$R_{24} = R_{C2} + R_{channel24}(\alpha_2) + R_{C4},$$

where $R_{C1} \ldots R_{C4}$ are the contact resistances and $R_{channel13}(\alpha_1)$ and $R_{channel24}(\alpha_2)$ denote the resistance of 200 μm × 600 μm graphene channels. It was assessed with additional TLM (*Transfer Length Method*) structures featuring 200 μm × 200 μm pads located next to the equal-arm crosses that the unit length contact resistance varied between 600 Ωμm and 1100 Ωμm, indicating that a single 200 μm × 200 μm contact pad introduces between 3 Ω and 5.5 Ω. In order to verify possible angle dependence of the contact resistance, the TLM structures were fabricated at a range of angles with respect to SiC terraces and multiplied for each orientation, so that the results had a statistical perspective. In the analyzed sample, these angles lied in the range between 40° and 90°. The experimental values proved no angle dependence (Fig. 2). The authors believe that in any given cross R_{C1} and R_{C3}, as well as R_{C2} and R_{C4} are mutually approximately equal and their difference is negligible with respect to the expected value of $R_{channel13}(\alpha_1)$ - $R_{channel24}(\alpha_2)$.

Based on the measured values of R_{13} and R_{24}, one can calculate the following relation:

$$\Delta R(\Delta\alpha) = |R_{13} - R_{24}|, \quad \text{where} \quad \Delta\alpha = |\alpha_1 - \alpha_2|$$

$\Delta R(\Delta\alpha)$ reflects the differential resistance between two perpendicular graphene channels as a function of the differential angle $\Delta\alpha$. For $\alpha_1 = \alpha_2 = 45°$ and $\Delta\alpha = 0$, which holds for identical terrace orientation in both channels, $\Delta R(\Delta\alpha)$ is expected to account for zero. When $\Delta\alpha = 90°$, $\Delta R(\Delta\alpha)$ reaches its maximum value and equals the excess resistance introduced by a finite number of SiC step edges that are 200 μm wide and cover the entire graphene channel. The authors chose to locally define a $\Delta R(\Delta\alpha)$ relation for each of the equal-arm crosses to minimize possible influence of graphene's quality inhomogeneity that if occurred throughout the sample would interfere with the influence of SiC step edges. The nine Hall crosses provide nine data points for a linear fit that reproduces the $\Delta R(\Delta\alpha)$ relation. We later use this fitted relation in the form of $y = ax + b$ to calculate the exact value of

$$\Delta R(\Delta\alpha = 90°) = a \times 90° = n_{edges} \times \rho_{step}/200\,\mu\text{m}, \qquad (1)$$

where n_{edges} is the number of SiC step edges. The intercept b is intentionally neglected as it is attributed other than terrace origin, however the authors cannot provide a meaningful explanation for its origin. The accurate number of SiC step edges n_{edges} over the distance of 600 μm is specific for each sample and was determined with the use of an atomic force microscope. Based on $a \times 90° = n_{edges} \times \rho_{step}/200\,\mu\text{m}$, the average resistivity ρ_{step} [Ωμm] of a single SiC step edge in QFS-bilayer graphene was derived.

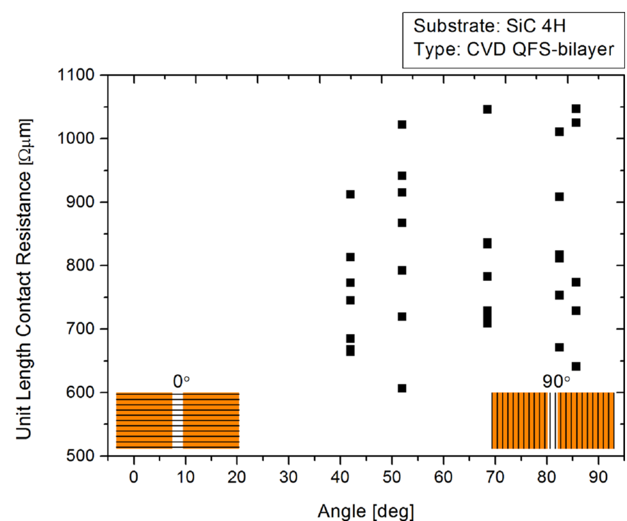

FIG. 2. Statistical analysis of the unit length contact resistance angle dependence measured in TLM structures featuring 200 μm × 200 μm contact pads. The TLM structures were rotated at different angles with respect to SiC terraces and multiplied to illustrate possible data distribution for the same angle. The insets schematically illustrate the terrace orientation between two adjacent TLM pads and the adopted convention for angle assignment.

[This article is copyrighted as indicated in the article. Reuse of AIP content is subject to the terms at: http://scitation.aip.org/termsconditions. Downloaded to] IP: 139.179.58.12 On: Thu, 25 Dec 2014 09:28:58

III. EXPERIMENTAL RESULTS

The qualitative observation of the step-edge-induced resistance anisotropy in hydrogen intercalated graphene on 4H-SiC(0001) and 6H-SiC(0001) (10 mm × 10 mm) substrates is presented in Figs. 3(a) and 3(b), respectively. The convention for the angle assignment of the terraces orientation with respect to the sample edges was depicted in Fig. 1(a). The $R_{VERTICAL}/R_{AVERAGE}$ and $R_{HORIZONTAL}/R_{AVERAGE}$ data points, where $R_{VERTICAL}$ and $R_{HORIZONTAL}$ are the auxiliary *van der Pauw* resistances and $R_{AVERAGE}$ is a hypothetical quantity that corresponds to R_S through $2exp(-\pi R_{AVERAGE}/R_S)=1$, clearly illustrate the cumulative effect of SiC step edges on the total resistance of QFS-bilayer graphene. The lowest normalized resistance is observed in the direction parallel to the SiC terraces ($\alpha = 0°$ for $R_{HORIZONTAL}/R_{AVERAGE}$ and $\alpha = 90°$ for $R_{VERTICAL}/R_{AVERAGE}$). It gradually increases as the step edges effectively hinder the current flow. In the direction perpendicular to the terraces, the normalized resistance reaches its maximum ($\alpha = 90°$ for $R_{HORIZONTAL}/R_{AVERAGE}$ and $\alpha = 0°$ for $R_{VERTICAL}/R_{AVERAGE}$). Both datasets are mutually symmetrical and cross exactly at the angle of 45°, which is in agreement with the expectations. Qualitatively similar results are obtained for 4H-SiC and 6H-SiC substrates. It happened that within the set of 60 6H-SiC samples, a majority displayed terraces oriented along the substrate's edges, hence an accumulation of data points around 5° and 85°. The significantly larger spread of resistance values at these angles as compared with intermediate steps is explained by the fact that within a more numerous set, one encounters a wider distribution of the total number of terraces, which translates into the observable data span. The statistical analysis of 200 samples proves that the step edges constitute a non-negligible mechanism of carrier transport impediment.

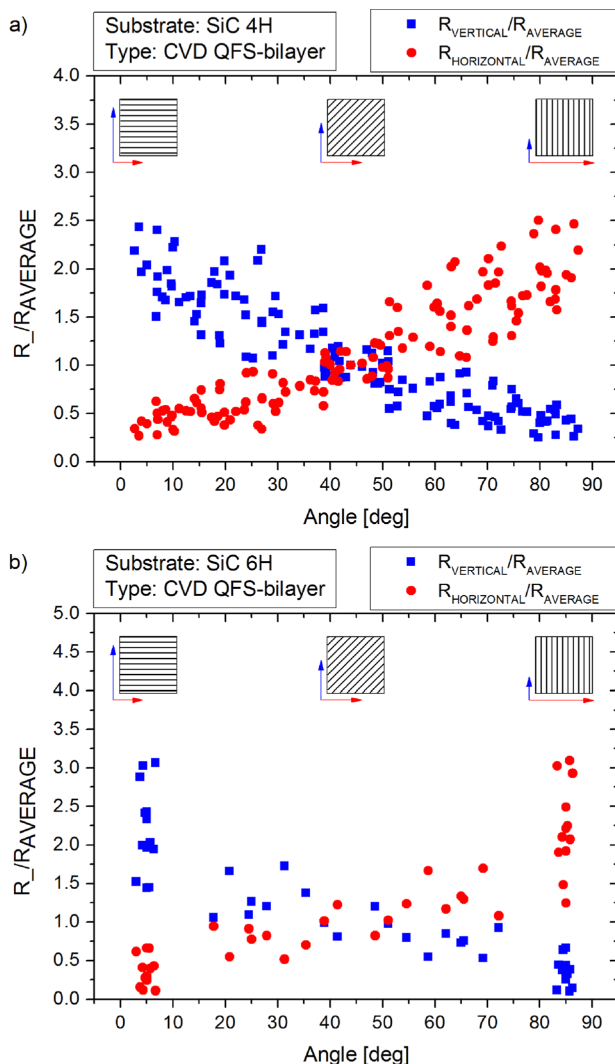

FIG. 3. The qualitative observation of the resistance anisotropy ($R_{VERTICAL}/R_{AVERAGE}$ and $R_{HORIZONTAL}/R_{AVERAGE}$) in the function of the terraces orientation with respect to the sample edges in CVD QFS-bilayer graphene measured in *van der Pauw* geometry on the surface of 10 mm × 10 mm samples. (a) 4H-SiC(0001) and (b) 6H-SiC(0001).

The quantitative description of the average step edge resistivity ρ_{step} is brought by the Hall crosses rotated at a varying angle with respect to SiC terraces (Fig. 1(b)). The measured $\Delta R(\Delta\alpha)$ relation of the two hydrogen intercalated 4H-SiC samples is depicted in Fig. 4. ΔR is the differential resistance between two perpendicular graphene channels and $\Delta\alpha$ is the differential angle between the terraces orientation in the two channels. It is expected that when $\alpha_1 = \alpha_2 = 45°$ and $\Delta\alpha = |\alpha_1 - \alpha_2| = 0$, which holds for identical terraces orientation in both channels, ΔR should equal 0 and reach its maximum for $\Delta\alpha = 90°$, when in one channel, the terraces run parallel to the direction of the current flow and perpendicular in the other. It was observed that for every $\alpha_1 < \alpha_2$, $R_{13} > R_{24}$, and $R_{13} < R_{24}$ for $\alpha_1 > \alpha_2$. This is indicative of the step-edge-induced resistance anisotropy and it is consistent with the above reported qualitative observation that the more terraces hamper the current flow the higher the resistance. The collected data points were linear fitted with $y = ax + b$ and yield the slope a equal to 0.915 and 1.393. Contrary to expectations for $\Delta\alpha = 0$, the intercept $b \neq 0$ ($\Delta R \neq 0$). We attribute it other than terrace origin and intentionally neglect in the determination of ρ_{step}. Both samples were inspected

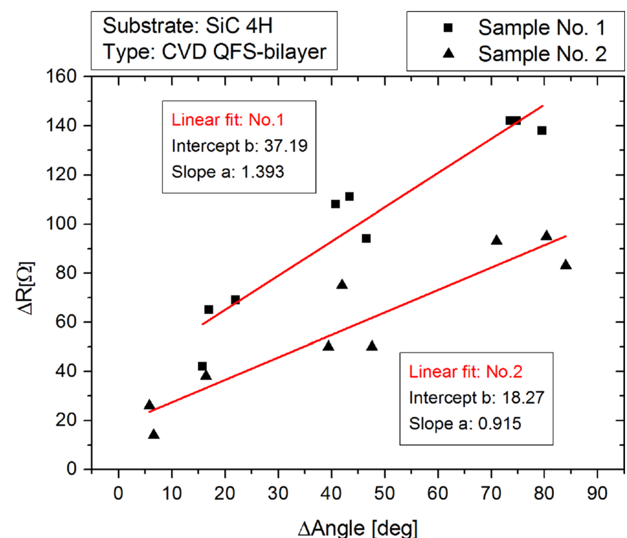

FIG. 4. Differential resistance ΔR measured in nine pairs of mutually perpendicular graphene channels (200 μm × 600 μm) as a function of the differential angle $\Delta\alpha$ between the terraces orientation in each pair of the mutually perpendicular channels fabricated on two QFS-bilayer 4H-SiC(0001) samples.

[This article is copyrighted as indicated in the article. Reuse of AIP content is subject to the terms at: http://scitation.aip.org/termsconditions. Downloaded to] IP: 139.179.58.12 On: Thu, 25 Dec 2014 09:28:58

with a NanoScope Controller driven Veeco Dimension V atomic force microscope equipped with an OTESPA cantilever. A 2 mm-long line scan in the direction perpendicular to the terraces was performed in order to statistically define an average number of SiC step edges n_{edges} over the distance of 600 μm, which is the length of either of the graphene channels. The two samples were assigned $n_{edges} \sim 81$ and $\sim$130, respectively. Based on Eq. (1), the resultant step edge resistivity was calculated 203 $\Omega\mu$m and 192 $\Omega\mu$m, accordingly.

Given these, one can relate the calculated values of ρ_{step} to the observed qualitative anisotropy in graphene's resistance depicted in Fig. 3. For $\rho_{step} = 203\,\Omega\mu$m, $n_{edges} \sim 81$ over the distance of 600 μm, and sample dimensions 10 mm × 10 mm, the total additional resistance introduced by SiC step edges in the direction perpendicular to the current flow equals $R_{step} = \rho_{step} \cdot N_{edges}/W_{edges} = 203\,\Omega\mu\text{m} \cdot (10\,\text{mm} \cdot 81/600\,\mu\text{m})/10\,\text{mm} = 27.4\,\Omega$, where N_{edges} and W_{edges}, are the total number and width of step edges, respectively. In case of the second sample, $\rho_{step} = 192\,\Omega\mu$m, $n_{edges} \sim 130$, $R_{step} = 41.6\,\Omega$. These additional step-edge-induced resistances constitute $\sim$18% and $\sim$28% of average R_S of these samples ($\sim$150 Ω) measured in *van der Pauw* geometry. Such a contribution is less severe than it was predicted by Fig. 3, where it is suggested that over the area of 10 mm × 10 mm sample, the terraces introduce around 100% the average R_S. The authors believe that the overestimated anisotropy induced from *van der Pauw* characterization has its origin in the specificity of this technique itself. During the measurement, the current path spans only a fraction of the substrate's surface. It is narrower than the sample's width and its highest density is localized near the sample's edge between the two current contacts and thus it experiences relatively overestimated step-edge-induced resistance.

These derived resistivities ρ_{step} are higher than those discussed in Ref. 51, where for monolayer graphene, the following values were obtained: $\sim$7 $\Omega\mu$m for step height $h_S = 0.5$ nm, $\sim$15 $\Omega\mu$m for $h_S = 1.0$ nm, and $\sim$25 $\Omega\mu$m for $h_S = 0.5$ nm. Nearly identical resistivities for monolayer graphene were reported in Ref. 54. However, they imply atomic steps rather than macro steps that originate from step bunching. In this report, the calculated values of ρ_{step}, i.e., 203 $\Omega\mu$m and 192 $\Omega\mu$m correspond to step heights of $\sim$7.4 nm and $\sim$10.0 nm. These numbers come as an average step height measured with an atomic force microscope over a distance of 2 mm and are found to be symptomatic for the step bunching phenomenon. Typical values of step heights and terrace widths witnessed after the growth-preceding *in-situ* hydrogen etching of SiC surface are depicted in Fig. 5.

In Ref. 54, it was found that for monolayer graphene, the mechanical deformation of graphene sheet cannot account for the observed step edge resistivity and it is rather the abrupt variation in potential and doping due to the detachment of graphene from the substrate as it passes over a step that introduces the additional scattering mechanism. To support this reasoning, we investigated a monolayer CVD graphene transferred from copper onto the 4H-SiC substrate using the PMMA-mediated technique. To assure that the transferred graphene reproduces SiC surface morphology and the step edge curvature, we analyzed its bending over an etched pit dislocation. It has been confirmed using SEM imaging that graphene precisely imitates the substrate's texture. The nine rotated Hall bars were characterized accordingly to the procedure adopted for the two hydrogen intercalated 4H-SiC samples. No recognizable pattern in resistance anisotropy was detected (Fig. 6(c)). Unlike in CVD QFS-bilayer graphene grown on SiC, where for $\alpha_1 < \alpha_2$, $R_{13} > R_{24}$, and $R_{13} < R_{24}$ when $\alpha_1 > \alpha_2$, here the measured ΔR took random, both positive and negative values in the range of approximately $\pm$600 Ω. Bearing in mind the measured R_{ij} resistance between the opposite contact pads of approximately 3.8 kΩ − 8.2 kΩ, we state that ΔR is relatively weaker (<12% of R_{ij}) than it was witnessed for epitaxial QFS-bilayer graphene (ΔR up to 38% of R_{ij}, R_{ij} in the range of 370 Ω−710 Ω). Thus, taking into account the lower values of ΔR relative to R_{ij} and their random nature, we attribute the data scatter to inhomogeneities in local transport properties of the transferred graphene. This observation provides further proof that the step edge resistivity cannot originate from graphene's mechanical deformation. This conclusion suggests that the charge carriers are not subject to scattering

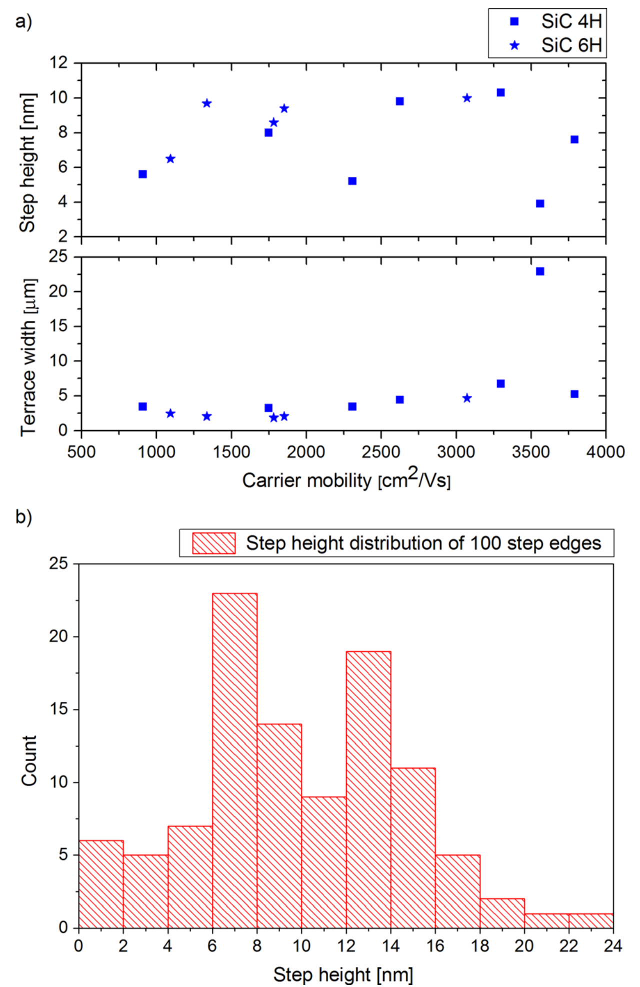

FIG. 5. (a) Typically witnessed average step heights and average terrace widths resulting from the step bunching phenomenon during the growth-preceding *in-situ* hydrogen etching of SiC surface (the reported values refer to 12 4H and 6H on-axis SiC samples and are averaged over a distance of 2 mm). (b) Exemplary step height distribution of the consecutive 100 SiC step edges.

[This article is copyrighted as indicated in the article. Reuse of AIP content is subject to the terms at: http://scitation.aip.org/termsconditions. Downloaded to] IP: 139.179.58.12 On: Thu, 25 Dec 2014 09:28:58

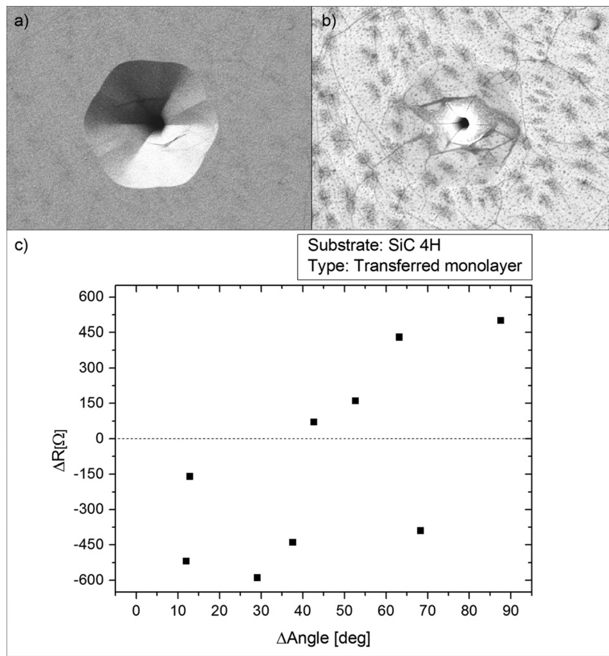

FIG. 6. (a) Scanning electron microscopy image of an etched pit dislocation ($4\,\mu$m in diameter) before and (b) after graphene transfer. Graphene's ability to reproduce surface morphology is proven by the smooth coverage of the pit slopes. (c) Differential resistance ΔR measured in nine pairs of mutually perpendicular graphene channels ($200\,\mu m \times 600\,\mu m$) as a function of the differential angle $\Delta\alpha$ between the terraces orientation in each pair of the mutually perpendicular channels in monolayer CVD copper-grown graphene transferred onto 4H-SiC(0001) substrate.

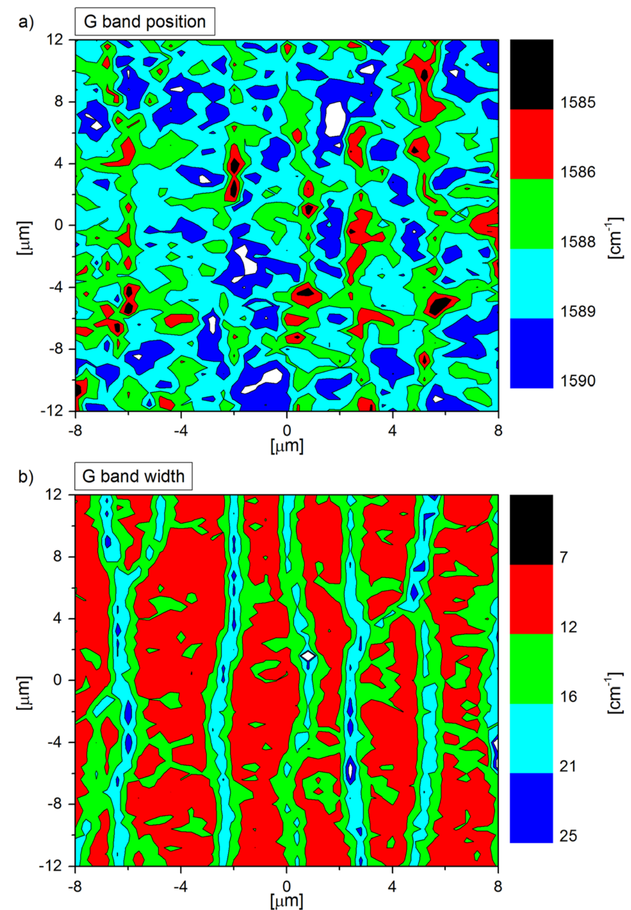

FIG. 7. Micro-Raman $24\,\mu m \times 16\,\mu m$ map of QFS-bilayer epitaxial CVD graphene on SiC. (a) G band position and (b) G band width.

over the substrates steps and consequently the step edge area does not influence their mobility. Bearing in mind that the resistance is a product of both carrier mobility μ and concentration n ($R^{-1} = en\mu$), we conclude that the derived ρ_{step} may originate from a decreased carrier population in the step area.

The possible carrier population depletion is expected to manifest itself in Raman spectroscopy imaging of the terrace and step edge area.[62] Micro-Raman $24\,\mu m \times 16\,\mu m$ maps of a hydrogen intercalated QFS-bilayer graphene within the terrace and step edge area, performed in a backscattering geometry using an inVia Renishaw microscope powered by a 532 nm CW Nd-YAG laser, are depicted in Figs. 7 and 8.

The number of graphene layers is verified in two ways. First, the FWHM of the 2D band within the terrace area is $\sim$60 cm^{-1} and it reaches $\sim$70 cm^{-1} on the step edges (Fig. 8(b)). It has been shown that exfoliated bilayer graphene exhibits a 2D FWHM of $\sim$50 cm^{-1} (Ref. 63) and other reports yield a range of 41–60 cm^{-1}.[64–68] Therefore, we reason that the terraces are covered with bilayer graphene and that there is an additional graphene layer in the step edge area. Second, bilayer graphene is expected to yield an asymmetric 2D band that is only reproduced by a sum of four Lorentzians, whereas the 2D band of a trilayer graphene is symmetrical and may by approximated by a single Voigt curve. Following the procedure adopted in Ref. 69, we analyze the overall quality of fitting the measured 2D band with a set of four Lorentzian curves and with a single Voigt function. An exemplary Raman spectrum within the terrace and step edge area is presented in Fig. 9. The comparison of the *chi-squared* value of the fitting correctness of the 2D band with the above mentioned functions (Figs. 10(a) and10(b)) proves that the terrace area is better approximated with a four-fold Lorentzian whereas the step edge area by a single Voigt, which suggests that the step edges are decorated with an additional (third) graphene layer.

In Ref. 70, it was clearly presented that under biaxial strain conditions, when the position of the G band in bilayer graphene is rising, the position of the 2D band is also increased. This is in contrast to the step edges, where an observable blue-shift of the 2D band is followed by a red-shift of the G band (Figs. 8(a) and 7(a)). We attribute the mechanism responsible for the blue-shift of the 2D band predominantly to strain induced by the step edges. Taking into account the fact that a deviation from a consistent shift of the G band and 2D band positions is mostly an evidence of carrier concentration changes and that in our experiment the red-shift of the G band position (Fig. 7(a)) is followed by a sharp increase in its width (Fig. 7(b)),[71] we reason from the Raman results that carrier concentration is lowered at the step edges as compared with the terraces.

It is assumed in Ref. 54 that along the detachment length $l_d \approx 1.2h_S$, where h_S is the step height, graphene is fully depleted of carriers. As a result, the step edge resistivity is expected to scale linearly with the step height. In our

[This article is copyrighted as indicated in the article. Reuse of AIP content is subject to the terms at: http://scitation.aip.org/termsconditions. Downloaded to] IP: 139.179.58.12 On: Thu, 25 Dec 2014 09:28:58

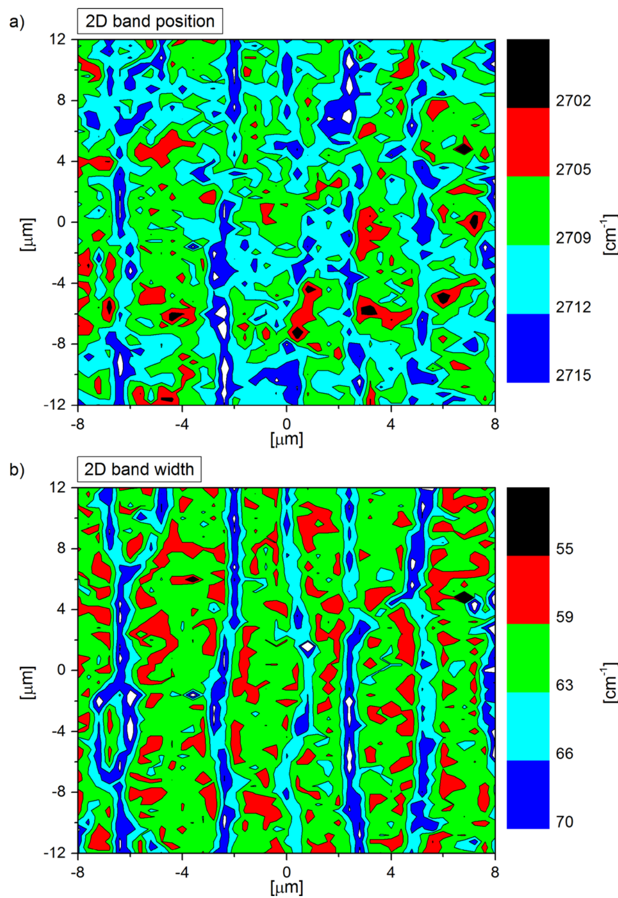

FIG. 8. Micro-Raman 24 μm × 16 μm map of QFS-bilayer epitaxial CVD graphene on SiC. (a) 2D band position and (b) 2D band width.

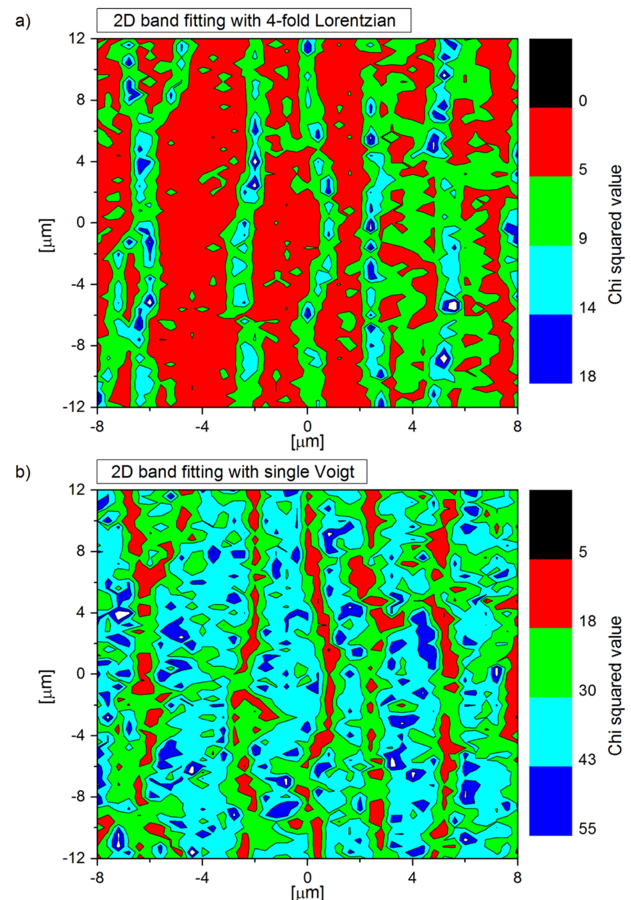

FIG. 10. Micro-Raman 24 μm × 16 μm map of QFS-bilayer epitaxial CVD graphene on SiC. (a) Residual error of 2D band fit with a 4-fold Lorentzian. (b) Residual error of 2D band fit with a single Voigt function.

experiment, the linear scaling is only supported for the orderly oriented terraces (Fig. 11). It has been observed that the meandering geometry promoted a ~50% higher step edge resistivity than it was expected for given h_S. On the basis of the fine agreement of our result derived for the orderly oriented terraces with the linear approximation of the reported data, we conclude that the adopted explanation for ρ_{step} origin is reliable. Yet, the overestimated step edge

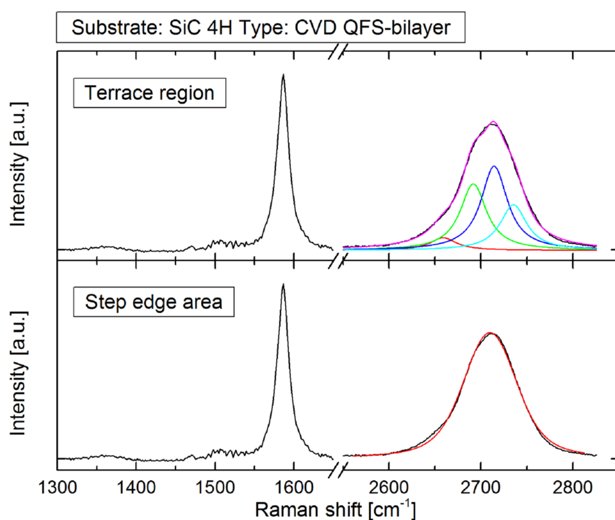

FIG. 9. Exemplary Raman spectrum within the terrace and step edge area. (a) In the terrace region, the 2D band is better approximated by a sum of four Lorentzian curves. (b) In the step edge area, the 2D band is better approximated by a single Voigt function.

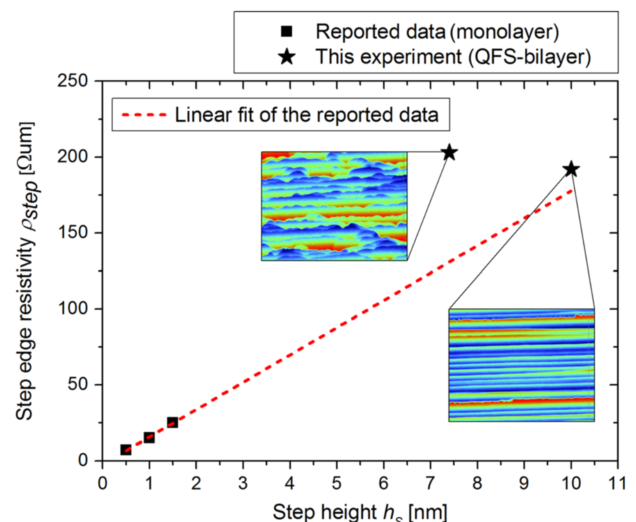

FIG. 11. Comparison of the reported values[51,54] of the step edge resistivity related to SiC atomic steps with our results for ρ_{step} indicative of the step bunching occurring during the growth-preceding *in-situ* hydrogen etching of the SiC surface. Inset imaging obtained with a Bruker ContourGT-I 3D optical microscope depicts surface morphology of the investigated samples (meandering and orderly oriented terraces).

[This article is copyrighted as indicated in the article. Reuse of AIP content is subject to the terms at: http://scitation.aip.org/termsconditions. Downloaded to] IP: 139.179.58.12 On: Thu, 25 Dec 2014 09:28:58

resistance of the winding terraces may suggest that graphene's resistance is further augmented by local morphology. Such contribution could be a consequence of residual Si atoms aggregated in the step edge area[55] or growth disorder near the step edges leading to deterioration of graphene's quality and promoting short-range scattering.[72]

IV. CONCLUSIONS

We showed the qualitative influence of SiC step edge orientation on the resistance of hydrogen intercalated QFS-bilayer graphene grown on 4H-SiC(0001) and 6H-SiC(0001) ($10\,mm \times 10\,mm$) by chemical vapor deposition. The statistical overview of 200 samples marks a distinctive relation between terrace orientation and the excess resistance. Similar results are observed for 4H and 6H polytypes. A further detailed analysis yields exact values of step edge resistivity in QFS-bilayer graphene on 4H-SiC substrate $\rho_{step} = 203\,\Omega\mu m$ for $h_S = 7.4\,nm$ and $\rho_{step} = 192\,\Omega\mu m$ for $h_S = 10.0\,nm$. In the case of orderly oriented terraces, our result is in agreement with the previously reported values for the step-height-scaling resistivity in monolayer graphene. It was observed that the meandering geometry of the terraces promoted a $\sim$50% higher step edge resistivity than it was expected for given h_S. No clear pattern was observed in the resistance anisotropy of the copper-grown graphene transferred onto a 4H-SiC substrate that would indicate the deformation-induced step edge resistivity. The results suggest that the adopted explanation for ρ_{step} origin, graphene's depletion of carriers over the detachment length, is reliable but this effect may be further augmented by growth disorder near the step edges and consequent short-range scattering. The authors believe that the typical macro step height ($\sim$10 nm) arising from the step bunching promoted by the *in situ* hydrogen etching of the SiC substrate gives rise to a non-negligible carrier transport impediment and should be considered in the design of the micro-scale graphene-based devices. In our analysis, we focused on large-scale, statistical parameters that will foster the reproducibility and standardization of the academic-scale technology and provide basis for the scalable, industrial, high-yield graphene production for electronics and sensor technologies.

ACKNOWLEDGMENTS

The authors thank Professor Jacek Baranowski for many useful discussions. The research leading to these results has received funding from the European Union Seventh Framework Programme under Grant Agreement No. 604391 Graphene Flagship. This work was also partially supported by the National Centre for Research and Development under the GRAF-TECH/NCBiR/01/32/2012 "GRAFMET" grant and GRAF-TECH/NCBiR/12/14/2013 "GRAFMAG" grant, the Ministry of Science and Higher Education under the Iuventus Plus 0296/IP2/2013/72 grant and the National Science Centre under the PRELUDIUM 2013/11/N/ST3/04147 grant.

[1] P. Avouris, "Graphene: Electronic and photonic properties and devices," Nano Lett. **10**, 4285 (2010).
[2] Y.-M. Lin, A. Valdes-Garcia, S.-J. Han, D. B. Farmer, I. Meric, Y. Sun *et al.*, "Wafer-scale graphene integrated circuit," Science **332**, 1294–1297 (2011).
[3] L. Wang, I. Meric, P. Y. Huang, Q. Gao, Y. Gao, H. Tran, T. Taniguchi, K. Watanabe *et al.*, "One-dimensional electrical contact to q two-dimensional material," Science **342**, 614 (2013).
[4] A. K. Geim and K. S. Novoselov, "The rise of graphene," Nature Mater. **6**, 183–191 (2007).
[5] S. Novoselov, A. K. Geim, S. V. Morozov, D. Jiang, Y. Zhang, S. V. Dubonos *et al.*, "Electric field effect in atomically thin carbon films," Science **306**, 666–669 (2004).
[6] Y. Zhang, J. W. Tan, H. L. Stormer, and P. Kim, "Experimental observation of the quantum Hall effect and Berry's phase in graphene," Nature **438**, 201–204 (2005).
[7] V. E. Dorgan, A. Behnam, H. J. Conley, K. I. Bolotin, and E. Pop, "High-field electrical and thermal transport in suspended graphene," Nano Lett. **13**, 4581–4586 (2013).
[8] K. I. Bolotin, K. J. Sikes, Z. Jiang, M. Klima, G. Fudenberg, J. Hone, P. Kim, and H. L. Stormer, "Ultrahigh electron mobility in suspended graphene," Solid State Commun. **146**, 351–355 (2008).
[9] X. Du, I. Skachko, A. Barker, and E. Y. Andrei, "Approaching the ballistic transport in suspended graphene," Nat. Nanotechnol. **3**, 491–495 (2008).
[10] T. Ando, "Screening effect and impurity scattering in monolayer graphene," J. Phys. Soc. Jpn. **75**, 074716 (2006).
[11] K. Nomura and A. H. MacDonald, "Quantum transport of massless Dirac fermions," Phys. Rev. Lett. **98**, 076602 (2007).
[12] V. V. Cheianov and V. I. Fal'ko, "Friedel oscillations, impurity scattering, and temperature dependence of resistivity in graphene," Phys. Rev. Lett. **97**, 226801 (2006).
[13] E. H. Hwang, S. Adam, and S. Das Sarma, "Carrier transport in two-dimensional graphene layers," Phys. Rev. Lett. **98**, 186806 (2007).
[14] S. Adam, E. H. Hwang, V. M. Galitski, and S. Das Sarma, "A self-consistent theory for graphene transport," Proc. Natl. Acad. Sci. U.S.A. **104**, 18392 (2007).
[15] D. S. Novikov, "Numbers of donors and acceptors from transport measurements in graphene," Appl. Phys. Lett. **91**, 102102 (2007).
[16] M. Trushin and J. Schliemann, "The minimum electrical and thermal conductivity of graphene: Quasiclassical approach," Phys. Rev. Lett. **99**, 216602 (2007).
[17] X.-Z. Yan, Y. Romiah, and C. S. Ting, "Electric transport theory of Dirac fermions," Phys. Rev. B **77**, 125409 (2008).
[18] J.-H. Chen, C. Jang, S. Adam, M. S. Fuhrer, E. D. Williams, and M. Ishigami, "Charged-impurity scattering in graphene," Nat. Phys. **4**, 377–381 (2008).
[19] W. Zhu, V. Perebeinos, M. Freitag, and P. Avouris, "Carrier scattering, mobilities, and electrostatic potential in monolayer, bilayer, and trilayer graphene," Phys. Rev. B **80**, 235402 (2009).
[20] D. B. Farmer, V. Perebeinos, Y.-M. Lin, C. Dimitrakopoulos, and P. Avouris, "Charge trapping and scattering in epitaxial graphene," Phys. Rev. B **84**, 205417 (2011).
[21] Y.-W. Tan, Y. Zhang, K. Bolotin, Y. Zhao, S. Adam, E. H. Hwang, S. Das Sarma, H. L. Stormer, and P. Kim, "Measurement of scattering rate and minimum conductivity in graphene," Phys. Rev. Lett. **99**, 246803 (2007).
[22] C. Jang, S. Adam, J.-H. Chen, E. D. Williams, S. Das Sarma, and M. S. Fuhrer, "Tuning the effective fine structure constant in graphene: Opposing effects of dielectric screening on short- and long-range potential scattering," Phys. Rev. Lett. **101**, 146805 (2008).
[23] D. S. Novikov, "Elastic scattering theory and transport in graphene," Phys. Rev. B **76**, 245435 (2007).
[24] S. Adam and S. Das Sarma, "Boltzmann transport and residual conductivity in bilayer graphene," Phys. Rev. B **77**, 115436 (2008).
[25] S. Das Sarma, E. H. Hwang, and E. Rossi, "Theory of carrier transport in bilayer graphene," Phys. Rev. B **81**, 161407 (2010).
[26] J. W. Klos and I. V. Zozoulenko, "Effect of short- and long-range scattering on the conductivity of graphene: Boltzmann approach vs tight-binding calculations," Phys. Rev. B **82**, 081414 (2010).
[27] S. Fratini and F. Guinea, "Substrate-limited electron dynamics in graphene," Phys. Rev. B **77**, 195415 (2008).
[28] V. W. Brar, Y. Zhang, Y. Yayon, T. Ohta, J. L. McChesney, A. Bostwick, E. Rotenberg, K. Horn, and M. F. Crommie, "Scanning tunneling spectroscopy of inhomogeneous electronic structure in monolayer and bilayer graphene on SiC," Appl. Phys. Lett. **91**, 122102 (2007).
[29] Y. Zhang, V. W. Brar, C. Girit, A. Zettl, and M. F. Crommie, "Origin of spatial charge inhomogeneity in graphene," Nat. Phys. Lett. **5**(10), 722–726 (2009).
[30] A. Castellanos-Gomez, R. H. M. Smit, N. Agrait, and G. Rubio-Bollinger, "Spatially resolved electronic inhomogeneities of graphene due to subsurface charges," Carbon **50**, 932–938 (2012).

[This article is copyrighted as indicated in the article. Reuse of AIP content is subject to the terms at: http://scitation.aip.org/termsconditions. Downloaded to] IP: 139.179.58.12 On: Thu, 25 Dec 2014 09:28:58

[31]K. Ziegler, "Robust transport properties in graphene," Phys. Rev. Lett. **97**, 266802 (2006).
[32]N. M. R. Peres, F. Guinea, and A. H. Castro Neto, "Electronic properties of disordered two-dimensional carbon," Phys. Rev. B **73**, 125411 (2006).
[33]E. A. Kim and A. H. Castro Neto, "Graphene as an electronic membrane," EPL **84**, 57007 (2008).
[34]M. I. Katsnelson and A. K. Geim, "Electron scattering on microscopic corrugations in graphene," Philos. Trans. R. Soc. A **366**, 195–204 (2008).
[35]H. Kuramochi, S. Odaka, K. Morita, S. Tanaka, H. Miyazaki, M. V. Lee, S.-L. Li, H. Hiura, and K. Tsukagoshi, "Role of atomic terraces and steps in the electron transport properties of epitaxial graphene grown on SiC,". AIP Adv. **2**, 012115 (2012).
[36]A. Fasolino, J. H. Los, and M. I. Katsnelson, "Intrinsic ripples in graphene," Nature Mater. **6**, 858–861 (2007).
[37]F. de Juan, A. Cortijo, and M. A. H. Vozmediano, "Charge inhomogeneities due to smooth ripples in graphene sheets," Phys. Rev. B **76**, 165409 (2007).
[38]I. F. Herbut, V. Juricic, and O. Vafek, "Coulomb interaction, ripples, and the minimal conductivity of graphene," Phys. Rev. Lett. **100**, 046403 (2008).
[39]J.-H. Chen, C. Jang, S. Xiao, M. Ishigami, and M. S. Fuhrer, "Intrinsic and extrinsic performance limits of graphene devices on SiO_2," Nat. Nanotechnol. **3**, 206–209 (2008).
[40]E. H. Hwang and S. Das Sarma, "Acoustic phonon scattering limited carrier mobility in two-dimensional extrinsic graphene," Phys. Rev. B **77**, 115449 (2008).
[41]S. V. Morozov, K. S. Novoselov, M. I. Katsnelson, F. Schedin, D. C. Elias, J. A. Jaszczak, and A. K. Geim, "Giant intrinsic carrier mobilities in graphene and its bilayer," Phys. Rev. Lett. **100**, 016602 (2008).
[42]Y.-M. Lin, C. Dimitrakopoulos, K. A. Jenkins, D. B. Farmer, H.-Y. Chiu, A. Grill, and Ph. Avouris, "100-GHz transistors from wafer-scale epitaxial graphene," Science **327**, 662 (2010).
[43]J. Hass, R. Feng, T. Li, X. Li, Z. Zong, W. A. de Heer, P. N. First, and E. H. Conrad, "Highly ordered graphene for two dimensional electronics," Appl. Phys. Lett. **89**, 143106 (2006).
[44]W. A. de Heer, C. Berger, M. Ruan, M. Sprinkle, X. Li, Y. Hu, B. Zhang, J. Hankinson, and E. Conrad, "Large area and structured epitaxial graphene produced by confinement controlled sublimation of silicon carbide," Proc. Natl. Acad. Sci. U.S.A. **108**, 16900–16905 (2011).
[45]C. Berger, J.-Y. Veuillen, L. Magaud, P. Mallet, V. Olevano, M. Orlita, and P. Plochocka, "Electronic properties of epitaxial graphene," Int. J. Nanotechnol. **7**, 383–402 (2010).
[46]W. Strupinski, K. Grodecki, A. Wysmolek, R. Stepniewski, T. Szkopek, and P. E. Gaskell, "Graphene epitaxy by chemical vapor deposition on SiC," Nano Lett. **11**(4), 1786–1791 (2011).
[47]K. V. Emtsev, A. Bostwick, K. Horn, J. Jobst, G. L. Kellogg, L. Ley, J. L. McChesney, T. Ohta, S. A. Reshanov, J. Röhrl, E. Rotenberg, A. K. Schmid, D. Waldmann, H. B. Weber, and T. Seyller, "Towards wafer-size graphene layers by atmospheric pressure graphitization of silicon carbide," Nature Mater. **8**, 203–207 (2009).
[48]M. J. Hollander, A. Agrawal, M. S. Bresnehan, M. LaBella, K. A. Trumbull, R. Cavalero, D. W. Snyder, S. Datta, and J. A. Robinson, "Heterogeneous integration of hexagonal boron nitride on bilayer quasi-free-standing epitaxial graphene and its impact on electrical transport properties," Phys. Status Solidi A **210**, 1062–1070 (2013).
[49]Y. Guo, L. W. Guo, J. Huang, R. Yang, Y. P. Jia, J. J. Lin, W. Lu, Z. L. Li, and X. L. Chen, "The correlation of epitaxial graphene properties and morphology of SiC (0001)," J. Appl. Phys. **115**, 043527 (2014).
[50]C. Dimitrakopoulos, A. Grill, T. McArdle, Z. Liu, R. Wisnieff, and D. A. Antoniadis, "Effect of SiC wafer miscut angle on the morphology and Hall mobility of epitaxially grown graphene," Appl. Phys. Lett. **98**, 222105 (2011).
[51]S.-H. Ji, J. B. Hannon, R. M. Tromp, V. Perebeinos, J. Tersoff, and F. M. Ross, "Atomic-scale transport in epitaxial graphene," Nature Mater. **11**, 114–119 (2011).
[52]S. E. Bryan, Y. Yang, and R. Murali, "Conductance of epitaxial graphene nanoribbons: Influence of size effects and substrate morphology," J. Phys. Chem. C **115**, 10230–10235 (2011).
[53]C. H. Lui, L. Liu, K. F. Mak, G. W. Flynn, and T. F. Heinz, "Ultraflat graphene," Nature **462**, 339–341 (2009).
[54]T. Low, V. Perebeinos, J. Tersoff, and Ph. Avouris, "Deformation and scattering in graphene over substrate steps," Phys. Rev. Lett. **108**, 096601 (2012).
[55]M. K. Yakes, D. Gunlycke, J. L. Tedesco, P. M. Campbell, R. L. Myers-Ward, C. R. Eddy, Jr., K. Gaskill, P. E. Sheehan, and A. R. Laracuente, "Conductance anisotropy in epitaxial graphene sheets generated by substrate interactions," Nano Lett. **10**, 1559–1562 (2010).
[56]N. Ray, S. Shallcross, S. Hensel, and O. Pankratov, "Buffer layer limited conductivity in epitaxial graphene on the Si face of SiC," Phys. Rev. B **86**, 125426 (2012).
[57]C. Riedl, U. Starke, J. Bernhardt, M. Franke, and K. Heinz, "Structural properties of the graphene-SiC(0001) interface as a key for the preparation of homogeneous large-terrace graphene surfaces," Phys. Rev. B **76**, 245406 (2007).
[58]K. V. Emtsev, F. Speck, Th. Seyller, L. Ley, and J. D. Riley, "Interaction, growth, and ordering of epitaxial graphene on SiC{0001} surfaces: A comparative photoelectron spectroscopy study: A comparative photoelectron spectroscope study," Phys. Rev. B **77**, 155303 (2008).
[59]C. Riedl, C. Coletti, T. Iwasaki, A. A. Zakharov, and U. Starke, "Quasi-free-standing epitaxial graphene on SiC obtained by hydrogen intercalation," Phys. Rev. Lett. **103**, 246804 (2009).
[60]L. J. van der Pauw, "A method for measuring the resistivity and Hall coefficient on lamellae arbitarty shape," Philips Res. Rep. **13**, 1–9 (1958).
[61]T. Ciuk, I. Pasternak, A. Krajewska, J. Sobieski, P. Caban, J. Szmidt, and W. Strupinski, "Properties of chemical vapor deposition graphene transferred by high-speed electrochemical delamination," J. Phys. Chem. C **117**, 20833–20837 (2013).
[62]K. Grodecki, R. Bozek, W. Strupinski, A. Wysmolek, R. Stepniewski, and J. M. Baranowski, "Micro-Raman spectroscopy of graphene grown on stepped 4H-SiC (0001) surface," Appl. Phys. Lett. **100**, 261604 (2012).
[63]A. C. Ferrari, J. C. Meyer, V. Scardaci, C. Casiraghi, M. Lazzeri, F. Mauri, S. Piscanec, D. Jiang, K. S. Novoselov, S. Roth, and A. K. Geim, "Raman spectrum of graphene and graphene layers," Phys. Rev. Lett. **97**(18), 187401 (2006).
[64]J. A. Robinson, M. Wetherington, J. L. Tedesco, P. M. Campbell, X. Weng, J. Stitt, M. A. Fanton, E. Frantz, D. Snyder, B. L. Vanmil, G. G. Jernigan, R. L. Myers-Ward, C. R. Eddy, Jr., and D. K. Gaskill, "Correlating Raman spectral signatures with carrier mobility in epitaxial graphene: a guide to achieving high mobility on the wafer scale," Nano Lett. **9**(8), 2873–2876 (2009).
[65]J. Röhrl, M. Hundhausen, K. V. Emtsev, Th. Seyller, R. Graupner, and L. Ley, "Raman spectra of epitaxial graphene on SiC(0001)," Appl. Phys. Lett. **92**(20), 201918 (2008).
[66]P. Lespade, A. Marchand, M. Couzi, and F. Cruege, Carbon **22**, 375 (1984).
[67]A. Ferrari and J. Robertson, "Interpretation of Raman spectra of disordered and amorphous carbon," Phys. Rev. B **61**, 14095 (2000).
[68]L. M. Malard, M. A. Pimenta, G. Dresselhaus, and M. S. Dresselhaus, "Raman spectroscope in graphene," Phys. Rep. **473**, 51–87 (2009).
[69]L. O. Nyakiti, R. L. Myers-Ward, V. D. Wheeler, E. A. Imhoff, F. J. Bezares, H. Chun, J. D. Caldwell, A. L. Friedman, B. R. Matis, J. W. Baldwin, P. M. Campbell, J. C. Culbertson, C. R. Eddy, Jr., G. G. Jernigan, and D. K. Gaskill, "Bilayer graphene grown on 4H-SiC (0001) step-free mesas," Nano Lett. **12**, 1749–1756 (2012).
[70]J. Zabel, R. R. Nair, A. Ott, T. Georgiou, A. K. Geim, K. S. Novoselov, and C. Casiraghi, "Raman spectroscopy of graphene and bilayer under biaxial strain: Bubbles and balloons," Nano Lett. **12**(2), 617–621 (2012).
[71]J. Yan, T. Villarson, E. A. Henriksen, Ph. Kim, and Aaron Pinczuk, "Optical phonon mixing in bilayer graphene with a broken inversion symmetry," Phys. Rev. B **80**, 241417 (2009).
[72]W. Strupinski, K. Grodecki, P. Caban, P. Ciepielewski, and J. M. Baranowski, "Formation mechanism of graphene buffer layer on SiC(0001)," Carbon (to be published).

[This article is copyrighted as indicated in the article. Reuse of AIP content is subject to the terms at: http://scitation.aip.org/termsconditions. Downloaded to] IP: 139.179.58.12 On: Thu, 25 Dec 2014 09:28:58